uc3m | Universidad Carlos III de Madrid
Department of Aerospace Engineering

IENAI [SPACE]

uc3m PHD

Near-Field Current Tomography for Spatially Resolved Emission Diagnostics in Multi-Emitter Electrospray Arrays

Maurizio Saggiani, Mick Wijnen, Jaume Navarro Cavallé
IENAI SPACE / Universidad Carlos III de Madrid

Motivation

Electrospray thrusters operate as distributed emission systems in which hundreds of emitters contribute simultaneously to total beam current. In an ideal array, each emitter operates under identical electrostatic and geometric conditions. In practice, manufacturing tolerances, bonding-induced misalignments, and local wetting variability introduce emitter-to-emitter differences that produce substantial spatial non-uniformity in current density.

Thrusters are commonly qualified using bulk electrical measurements: total emitted beam current , which represent only the spatial integral of the emission distribution. Fundamentally different emission states (uniform vs. clustered) can produce indistinguishable total current values. Classical diagnostics are therefore intrinsically blind to spatial emission structure.

Direct performance consequences: localised over-emission increases accelerates degradation; under-utilised regions reduce effective array efficiency; asymmetric emission induces plume misalignment and premature failure — even when total current remains nominal.

→ A diagnostic capable of resolving the spatial distribution of emitted current is required to bridge the gap between local emission physics and global thruster behaviour.

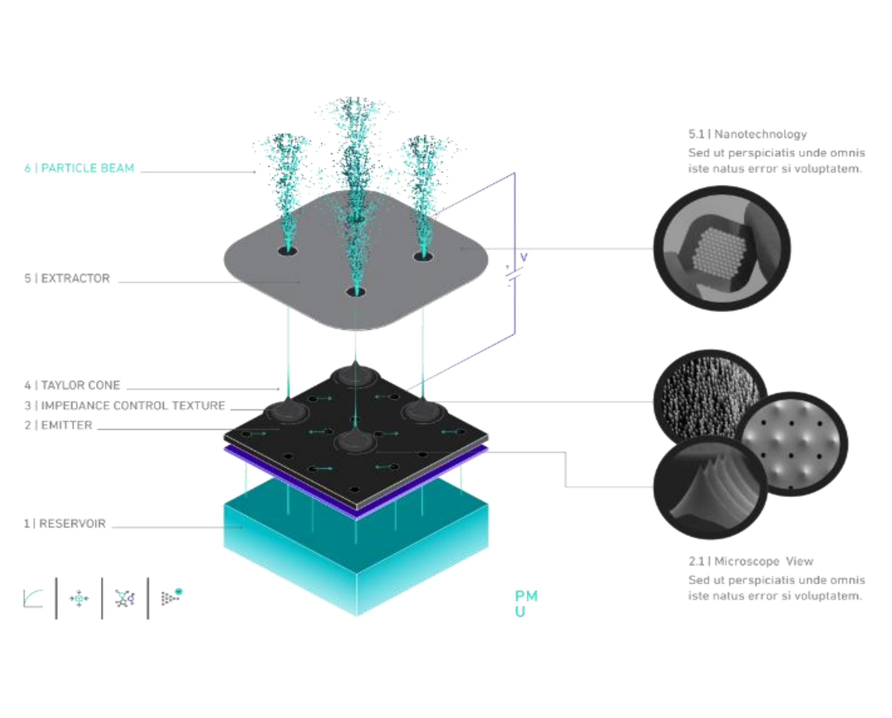

Electrospray thruster diagram

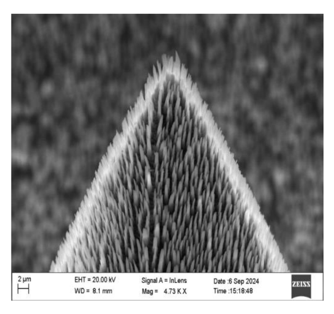

SEM image of one needle tip

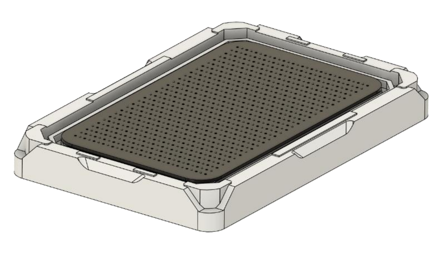

Array of 420 emission needles

State of the Art

Near-field current tomography (CT) uses wire-probe line-integrated current measurements to reconstruct the 2D current density distribution J(x,y) across the array via filtered backprojection (Fourier Slice Theorem).

Prior work: Courtney et al. (2019) established the CT geometric framework; Fedkiw et al. (2021) refined current mapping techniques; Villegas-Prados et al. (2024) extended CT to externally wetted architectures. These demonstrated qualitative capability to reveal non-uniformity.

Unresolved limitations: (1) Angular undersampling , no enforcement of the Nyquist sampling theorem applied to 2D periphery of the Fourier Space. (2) No quantitative validation — prior studies present CT maps without demonstrating that spatially integrated current recovers the independently measured I–V data. (3) No single emission site resolution.

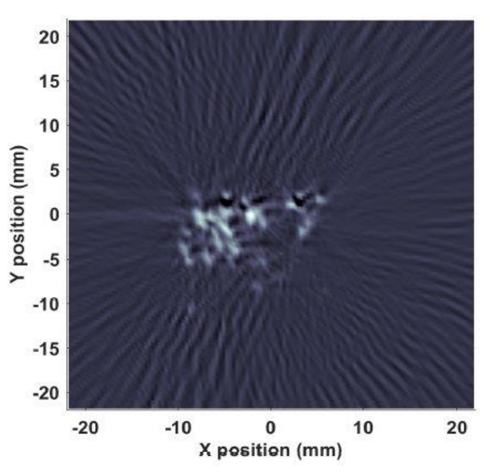

Courtney et al, 2019

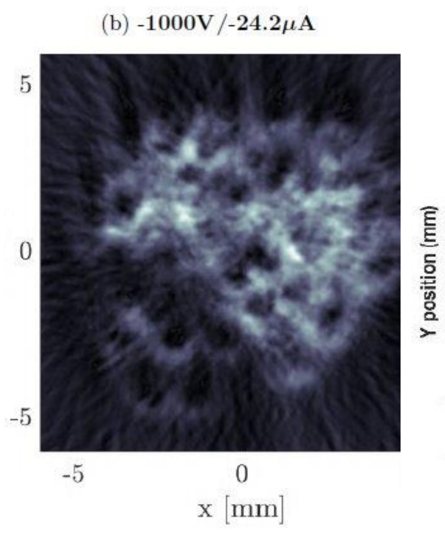

Villegas – Pardos et al, 2024

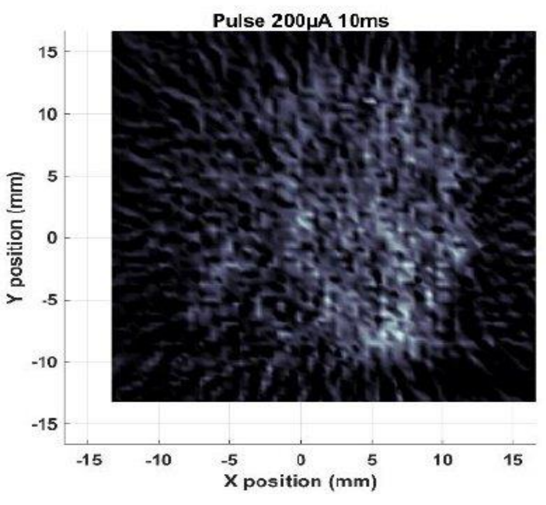

Fedkiw et al, 2021

Objectives

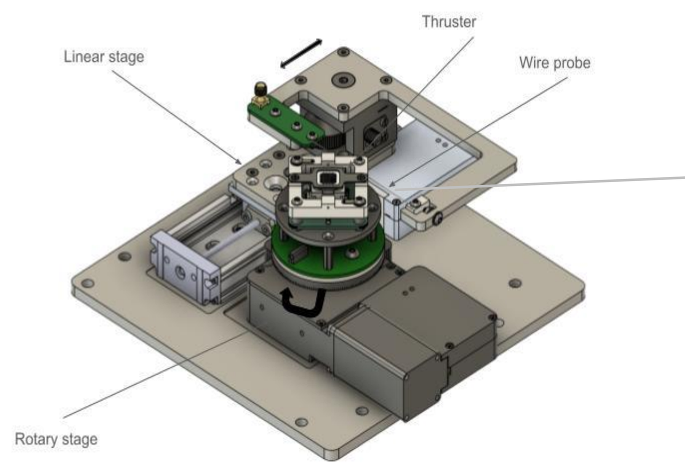

CT scanner assembly

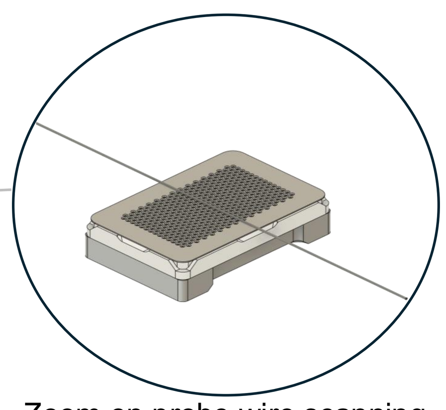

Zoom on probe wire scanning on top of the thruster

1. Enforce Nyquist-consistent sampling in CT reconstruction through projection-space radial binning, suppressing frequency-domain artifacts prior to filtered backprojection.
2. Resolving singular emission sites enforcing that the reconstruction pixel size is smaller than the needles interspacing area
3. Establish quantitative validation by demonstrating conservation of total emitted current: integrated CT current must close against independently measured I–V data.
4. Characterise emission non-uniformity in a 420-needle silicon array using CT, profilometry, and 2D electrostatic simulation, linking assembly geometry to spatial emission topology.

Methodology

For each angular position, the probe performs a linear sweep across the beam, recording the intercepted current. The collection of line-integrated measurements forms a **sinogram** p(r, θ).

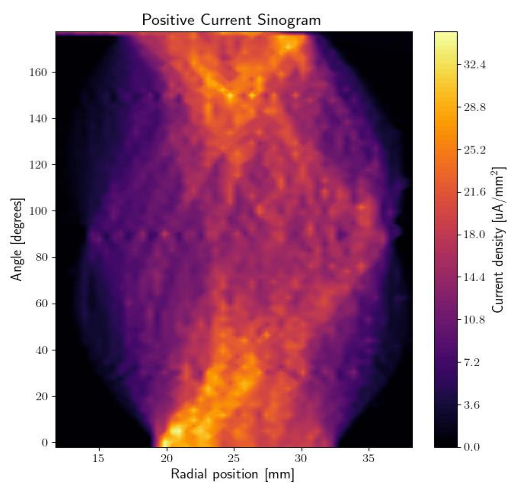

Filtered Backprojection is the dominant reconstruction algorithm for CT. It reconstructs an object function f(x,y) from the set of its line-integral projections p(r, θ) by filtering each projection with a ramp-shaped frequency filter and then backprojecting the result over the image plane. FBP falls directly out of rewriting the 2D inverse Fourier transform in polar coordinates (r, θ)

$$j(x,y) = \int_0^{\pi} Q_\theta\left(x\cos\theta + y\sin\theta\right) \mathrm{d}\theta$$

Where Q_θ is the FBP

Where the ω factor is the ramp filter

$$Q_\theta(t) = \int_{-\infty}^{+\infty} \mathcal{F}\{I(\cdot,\theta)\}(\omega)\,|\omega|\,e^{j2\pi\omega t}\,\mathrm{d}\omega$$

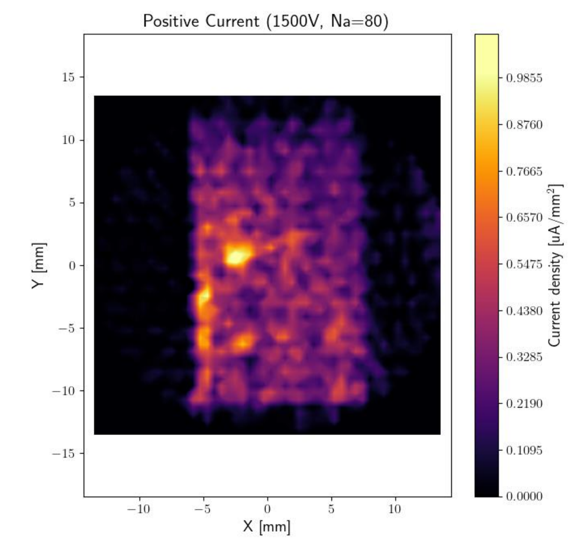

Frequency artifacts suppression and Single cone resolution

The sinogram is sampled in Fouries Space with the Radial frequency Nr and the Anguar frequency Nθ. In order to not encounter frequency resonances in the reconstruction of the image, we need to enforce the Nyquist sampling theorem adapted to 2D coupled variables and enforced at the periphery of the Fourier Space : **$N_\theta > (\pi/2) \cdot N_r$**

To resolve single emission sites we had to enforce that the reconstruction pixel is smaller than the inter-needle spacing area : **$\varepsilon = n_{needle} \cdot A_{px} < 1$** , where n_{needle} is the emission site spatial densiti and A_{px} the reconstruction pixel area

Quantitative validation – Integration Analysis

Integrating the current density J(i,j) over the entire array we were able to cross check total emitted current with the bulk classical collective data: when ε < 1 (no artifacts, single cone resolution) the predicted current match the bulk data with 1% error

$$I_{CT} = \sum_{i,j}^{n_{px}} J_{i,j} A_{px}$$

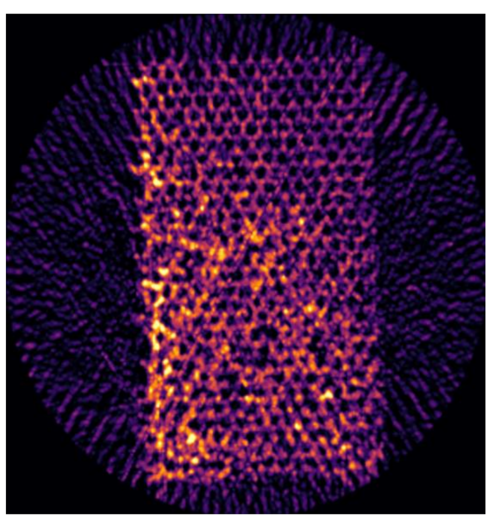

$N_\theta < (\pi/2) \cdot N_r$, ε > 1

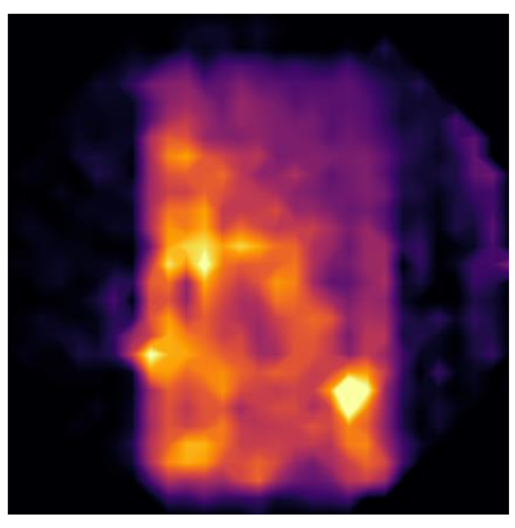

$N_\theta > (\pi/2) \cdot N_r$, ε > 1

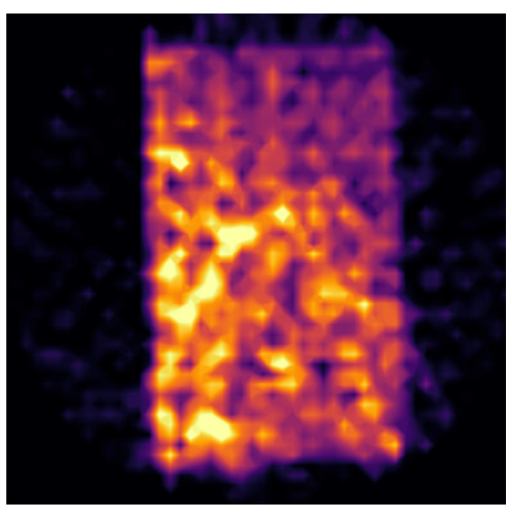

$N_\theta > (\pi/2) \cdot N_r$, ε < 1

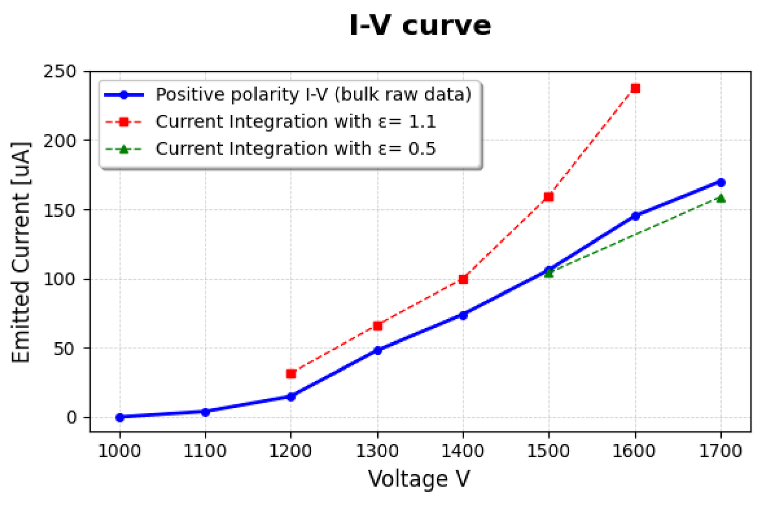

Quantitative validation

Preliminary Research/Results

Emission Heterogeneity

The reconstructed emission maps reveal two distinct classes of spatial heterogeneity: first a **distributed non-uniformity** component arising from emitter-to-emitter geometric and surface variability. Hotspots with 4x the average emission per site are now identified as clear lifetime and performance bottleneck. Secondly a systematic **large-scale gradient** persisting across all operating voltages indicating a macroscopic geometric or electrostatic driver, rather than stochastic manufacturing dispersion.

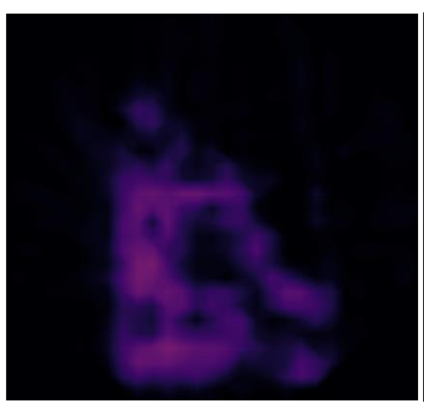

CT at 1200V

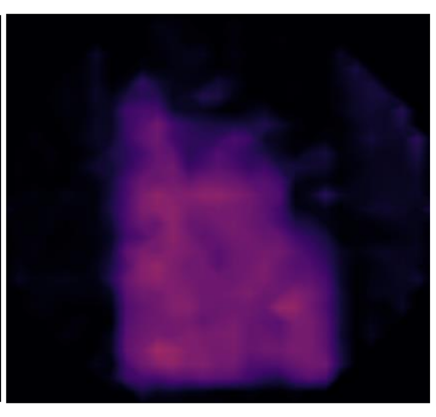

CT at 1300V

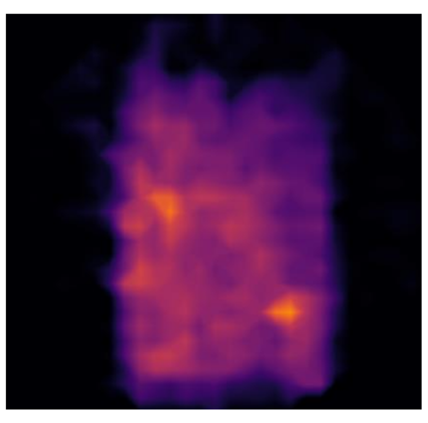

CT at 1400V

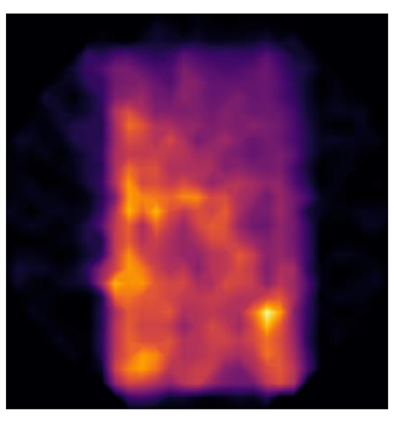

CT at 1500V

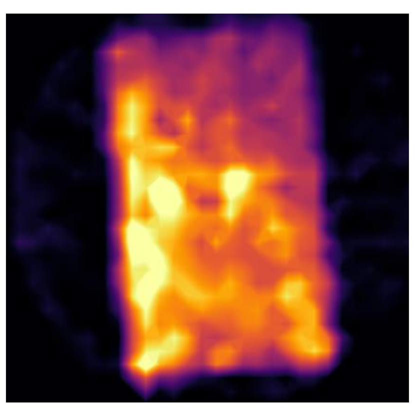

CT at 1600V

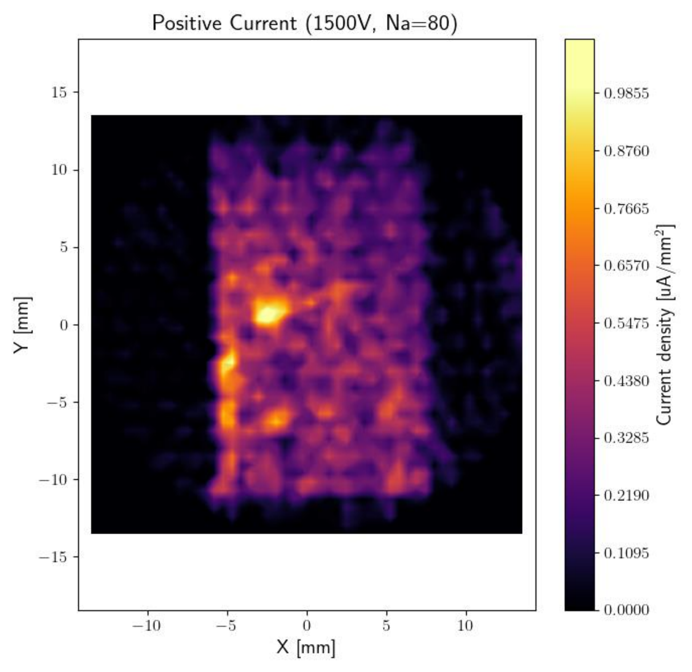

Distributed local hot spots and non uniformities.

Electrostatic Closure

With the aid of a 3D optical profilometry we found that the emitter array and the extractor plane (ideally parallel planes with a design gap g_0 = 150 μm) had a relative inclination of 0.1° per axis.The distribution of the gap (g) with the planes inclination was plotted over the entire array area. A 2D COMSOL finite element model electrostatic simulation of a cone-extractor, to compute the needle tip electric field in function of g, allowed us to predict the current density distribution J(x,y) in this scenario. Correlation with the CT image at the same voltage showed good correcaltion: The large scale gradiend is due to a 0.1° plane non-complanarity of emitetr and extractor planes. The distributed non uniformity due to emitter to emitter variability will be subject of further studies.

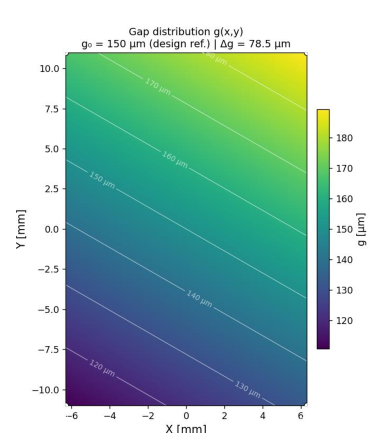

Emitter-extractor gap distribution

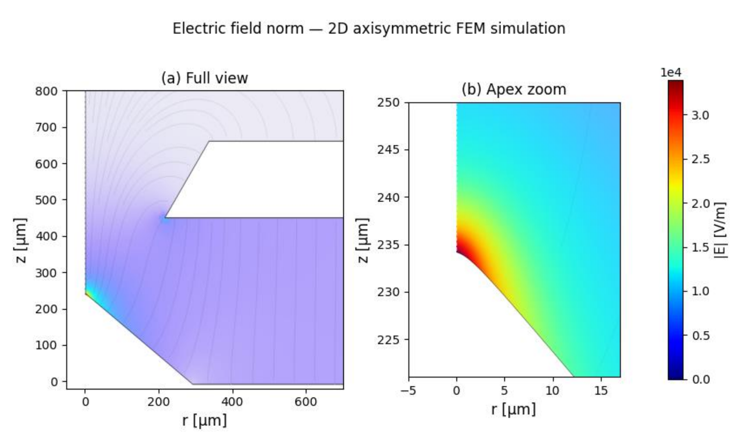

COMSOL electrostatatic simulation of tip electric field

Empirical scaling law:

$$J(x,y) = 0.839 \cdot \left(\frac{V - V_{onset}(x,y)}{V_{onset}(x,y)}\right)^{1.188}$$

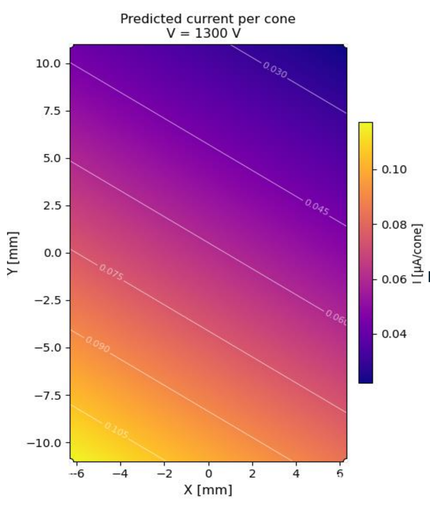

Simulated J(x,y) from gap distribution

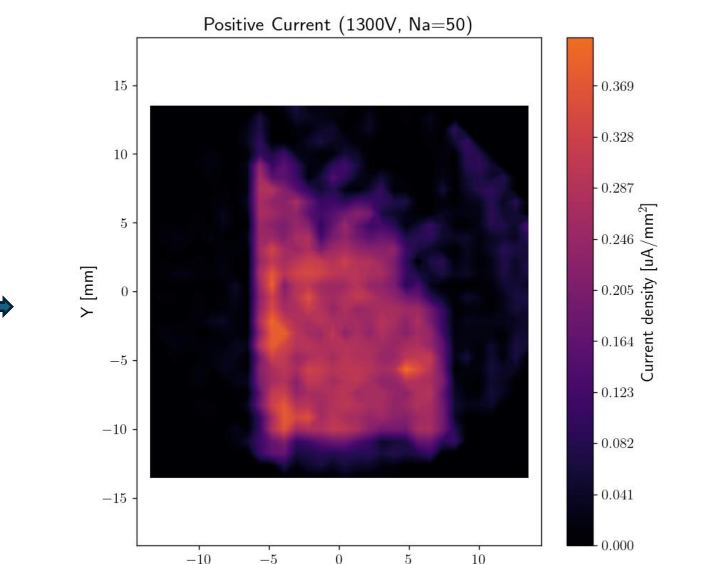

CT at 1300V

Aero space

PhD Student: Maurizio Saggiani – maurizio.saggiani@ienai.space
Supervisor: Jaume Navarro Cavallé – jaume.navarro@uc3m.es

IENAI [SPACE]